IEEE Photonics Journal
An IEEE Photonics Society Publication

Open Access

Low-Complexity Receiver Using Undersampling for Guard-Band SSB-DDO-OFDM

Volume 9, Number 4, August 2017

Ming Chen
Qinghui Chen
Hui Zhou
Zhiwei Zheng
Jing He
Lin Chen

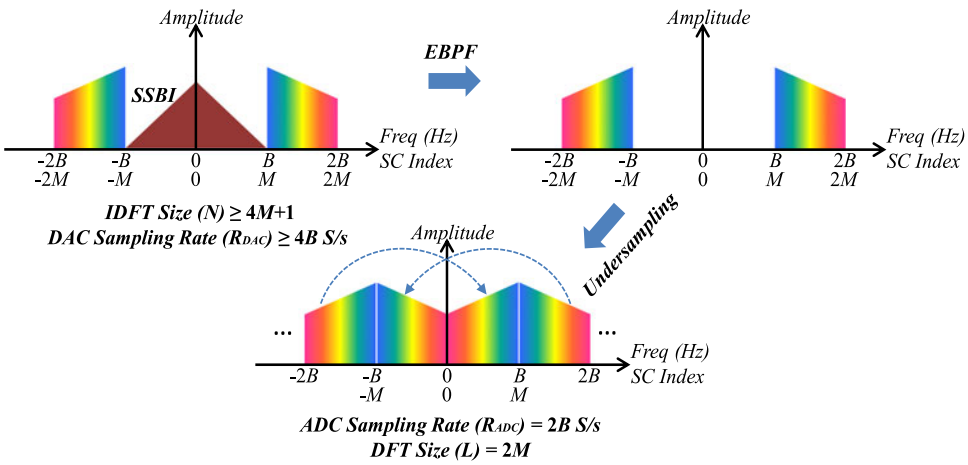

DOI: 10.1109/JPHOT.2017.2719045
1943-0655 © 2017 IEEE

IEEE photonics SOCIETY

IEEE

Low-Complexity Receiver Using Undersampling for Guard-Band SSB-DDO-OFDM

Ming Chen,[1] Qinghui Chen,[2] Hui Zhou,[1] Zhiwei Zheng,[1] Jing He,[2] and Lin Chen[2]

[1]College of Physics and Information Science, Hunan Normal University, Changsha 410081, China
[2]College of Computer Science and Electronic Engineering, Hunan University, Changsha 410082, China

DOI:10.1109/JPHOT.2017.2719045

Manuscript received May 17, 2017; revised June 19, 2017; accepted June 20, 2017. Date of publication June 23, 2017; date of current version July 11, 2017. This work was supported in part by the Hunan Provincial Natural Science Foundation of China under Grant 2017JJ3212, Grant 2016JJ6097, and Grant 14JJ6007, in part by the Scientific Research Fund of Hunan Provincial Education Department under Grant 14B119, and in part by the Project Supported for excellent talents in Hunan Normal University under Grant ET1502. Corresponding author: Ming Chen (e-mail: ming.chen@hunnu.edu.cn).

Abstract: A guard-band-based and single-side-band (SSB) modulation scheme is usually employed to improve receiver sensitivity and avoid power fading for the direct-detection optical orthogonal frequency-division multiplexing (DDO-OFDM). In this paper, we take advantages of analog-to-digital converter (ADC) undersampling to achieve a low-complexity receiver for guard-band SSB-DDO-OFDM. By using an electrical bandpass filter, the signal-to-signal beating interference is removed from the guard-band, and the desired OFDM signal is sampled at a rate twice its signal bandwidth rather than its highest frequency component. The guard-band will be filled with the aliased components which can be used to fully recover the transmitted data, and the discrete Fourier transform size at the receiver side is reduced by more than half. As a result, the implementation complexity of the receiver can be greatly reduced with the lower ADC sampling rate and reduced digital signal processing complexity. The feasibility of the proposed low-complexity receiver is investigated by numerical simulations. When the quantization noise is not dominant, the simulations show that the proposed low-complexity guard-band SSB-DDO-OFDM has similar error vector magnitude performances with the conventional one over different bias voltages and single-mode fiber links.

Index Terms: Undersampling, receiver sensitivity, guard band SSB-DDO-OFDM, signal-to-signal beating interference (SSBI).

1. Introduction

Direct-Detection optical orthogonal frequency-division multiplexing (DDO-OFDM) has been widely considered as one of the most promising candidates for cost-sensitive access applications, due to its simple configuration, great robustness to optical fiber dispersions and high spectral efficiency [1]–[4]. In recent years, DDO-OFDM has been extensively studied by both offline and real-time DSP approaches [5]–[12]. For most of the real-time DDO-OFDM systems, the input vector of the inverse

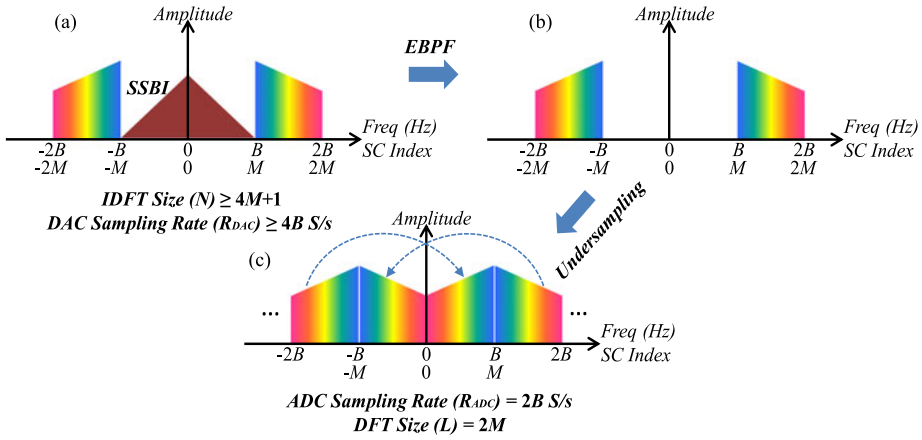

Fig. 1. The schematic diagram of the principle of the ADC sampling rate and DFT size reduction using undersampling.

discrete Fourier transform (IDFT) in the transmitter is constrained to have Hermitian symmetry (HS), which is regarded as a simple way to generate the real-valued OFDM signal for optical intensity modulation, while a single square-law photo-detector (PD) is used to recover the electrical OFDM signal in the receiver [7]–[12]. However, such a DDO-OFDM has poor receiver sensitivity due to high optical carrier-to-signal power ratio (CSPR) and inherent chromatic dispersion (CD)-induced power fading problem existed in double-side-band (DSB) modulation.

To improve the receiver sensitivity and avoid power fading, a guard-band based and single-side-band (SSB) modulated DDO-OFDM (SSB-DDO-OFDM) has been investigated by numerical simulation and experiments [1]–[3]. It concludes that a guard band between the optical carrier and the OFDM signal spectrum, with a bandwidth equal to the signal bandwidth (B), is needed to avoid the signal-to-signal beating interference (SSBI) due to the square-law photo-detection and obtain the best receiver sensitivity by applying an optimal DC bias voltage to the Mach-Zehnder modulator (MZM) [3]. Even though it's a spectrally-inefficient way to solve SSBI problem, the simpler system configuration or/and lower digital signal processing (DSP) complexity are achieved compared to other methods described in [13]–[16]. Adaptive modulation technique or high modulation formats can be employed to improve spectral efficiency. So we believe the guard-band SSB-DDO-OFDM may be more suitable for low-complexity hardware implementation.

However, the received OFDM signal is treated as a low-pass signal with a bandwidth of $2B$ and sampled at a rate equal to or greater than twice its highest frequency component, i.e., $4B$ samples per second (S/s), in the conventional guard-band SSB-DDO-OFDM, so the ADC works at an inefficient sampling rate. In this paper, to further reduce the implementation complexity of the guard-band SSB-DDO-OFDM, the received OFDM signal is regarded as a band-pass signal with a bandwidth of B, and then the aliasing effect due to the undersampling technique is applied to reduce the ADC sampling rate. The guard band will be filled with the aliased components which can be used to fully recover the transmitted data. Also, the discrete Fourier transform (DFT) size at the receiver side is reduced by more than half. As a result, the implementation complexity of the receiver can be greatly reduced with the lower ADC sampling rate and reduced DSP complexity.

This paper is arranged as follows. In Section 2, we describe in detail the principle of ADC sampling rate and DFT size reduction using the undersampling technique. The feasibility of the proposed low-complexity OFDM receiver is verified in the electrical back-to-back case in Section 3. In Section 4, the CSPR of the OSSB-OFDM signal generated by using MZM and optical filtering is theoretically analyzed. The simulation setup of the proposed guard-band SSB-DDO-OFDM is described in Section 5. In Section 6, the simulated results are presented and discussed. Conclusions are drawn in Section 7.

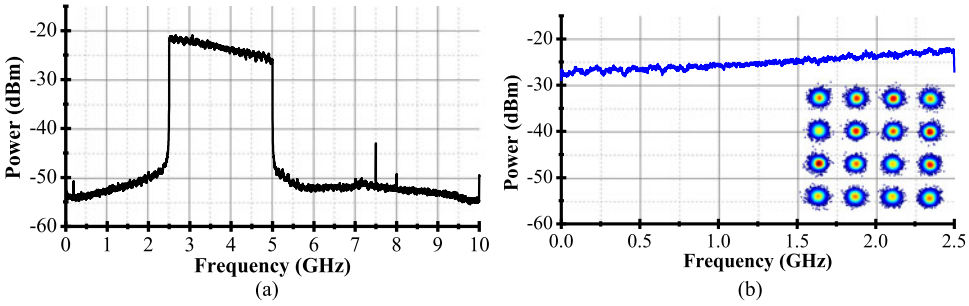

Fig. 2. Experimental measurements, (a) Power spectrum of the filtered OFDM signal; (b) Power spectrum of ADC captured samples (5 GS/s), and inset is the recovered 16-QAM constellation.

2. Principles of ADC Sampling Rate and DFT Size Reduction Using Undersampling

Fig. 1 shows the schematic diagram of the principle of the proposed low-complexity method using undersampling technique. The real-valued OFDM signal is generated by using Hermitian symmetric IDFT [8]. The IDFT size and data-carrying subcarriers (SCs) are N and M, respectively. M SCs around DC are filled with zeros for guard band with a bandwidth equals to the signal bandwidth (B), and (N-4M) SCs located at the high spectrum edge are used for oversampling. So N (DAC sampling rate, R_{DAC}) should equal to or greater than 4M (4B S/s). The optical SSB optical OFDM signal generated by using an optical band-pass filter after optical fiber transmission is directly-detected by a square-law PD. The spectral of the detected and filtered OFDM signals are schematically shown in Fig. 1(a) and (b), respectively. Here, the electrical band-pass filter (EBPF) is used to remove the SSBI.

The filtered OFDM signal is undersampled at a rate of 2B S/s, and the corresponding digital spectrum of the captured samples by using undersampling is presented schematically in Fig. 1(c). The relationship between the DFT size (L) and IDFT size is summarized as

$$\begin{aligned} L &= N \times R_{ADC}/R_{DAC} \\ &= N \times 2 \times B/R_{DAC} \\ &= N \times 2 \times (M \times R_{DAC}/N)/R_{DAC} \\ &= 2M < N/2 \end{aligned} \tag{1}$$

The relationship between IDFT inputs, $a_j, j \in [-N/2+1, N/2]$ and DFT outputs, $b_k, k \in [-M+1, M]$ can be expressed as

$$b_k = \begin{cases} a_{k+2M}, & k \in [-M+1, -1] \\ a_{-2M}+a_{2M}, & k = 0 \\ a_{k-2M}, & k \in [1, \quad M-1] \\ 0, & k = M \end{cases} \tag{2}$$

As we can see from Fig. 1(c), the aliased components containing all of the useful data modulated on M data-carrying SCs, which appear in the guard band according to Nyquist-Shannon sampling theorem. Therefore, the aliased components can be used to fully recover the transmitted data. It should be noted that the data on the DC SC, b_0, from 2M DFT outputs is real-valued, due to the superposition of two aliased components of two highest-frequency data-carrying SCs with indices of $\pm 2M$. This fact is the data on these two highest-frequency SCs are complex conjugated. So these two SCs can only be modulated with M-ary amplitude-shift keying (M-ASK) symbols.

As mentioned above, we can conclude that more than half of ADC sampling rate and DFT size is reduced by using the undersampling technique for the guard-band SSB-DDO-OFDM

TABLE 1
Some Parameters Used in the Experimental Measurements

Item	Parameter	Value	Unit
OFDM Frame	IDFT/DFT size (N/L)	4800/2000	-
	Data-carrying SCs	999	-
	Modulation format	16-QAM	-
	OFDM symbols per frame	100	-
	TSs per frame/ISFA taps	1/7	-
	CP length	12	points
	Digital clipping ratio (DCR)	13	dB
DAC	Sampling rate	12	GS/s
	Resolution	10	bits
ADC	Sampling rate	5	GS/s
	Resolution	8	bits
ELPF	3-dB Cutoff frequency	5.29	GHz

receiver. It can be used to reduce ADC cost and power consumption as well as the receiver DSP complexity.

3. Electrical Back-to-Back Measurements

To verify the feasibility of the proposed low-complexity receiver for guard-band SSB-DDO-OFDM, some experimental measurements mainly focusing on ADC undersampling at the electrical back to back (EBTB) case are conducted. The related results are presented in Fig. 2. One OFDM frame is offline generated and loaded into a Tektronix arbitrary waveform generator (AWG) with the model of AWG 7122C. The DAC located in the AWG is worked at a sampling rate of 12 GS/s. The bandwidth of the generated OFDM signal is 2.5 GHz, which equals to the bandwidth of the guard band [See Fig. 2(a)]. To remove DAC images, the generated OFDM signal is filtered by an ELPF and then sampled and stored by a digital storage oscilloscope (DSO, Teledyne Lecroy Wavemaster 820Zi-A) with an ADC operated at a sampling rate of 5 GS/s. A peak in the electrical spectrum is shown at the frequency of 7.5 GHz, which is the sampling clock noise [8]. The stored samples are post-processed by offline DSP algorithms as described in Section 5. The digital spectrum of the captured OFDM samples is plotted in Fig. 2(b), which is consistent with the spectrum shown in Fig. 1(c). The detailed parameters used in the experimental measurements are given in Table 1. The error vector magnitude (EVM) in dB can be expressed as [17], [18]

$$EVM = 20\log_{10}\left(\sqrt{\frac{1}{N_s}\sum_{k=1}^{N_s}|e_k|^2 \Big/ \frac{1}{N_s}\sum_{k=1}^{N_s}|X_k|^2}\right) \tag{3}$$

where X_k denotes the reference QAM symbol, Y_k is distorted version, N_s is the number of the transmitted QAM symbols, and $e_k = Y_k - X_k$ is the error signal. In this paper, N_s is 99,900.

The EVM of the recovered 16-QAM symbols as shown in Fig 2(b), which is calculated with 99,900 16-QAM symbols from 100 OFDM symbols, each containing 999 QAM symbols, is -21.6 dB. It indicates that the feasibility of the proposed method is verified in the electrical back to back case.

4. CSPR for Optical SSB-OFDM Signal

In this paper, an optical double-side-band (DSB) OFDM signal is generated with a single-drive MZM biased at a DC voltage close to its null point. The optical field at MZM output can be written as [19]

$$\begin{aligned} E_o(t) &\propto \cos\left(\frac{\pi}{2V_\pi}(s(t)+V_{bias})\right)\cos(2\pi f_c t) \\ &= \left[\cos\left(\frac{\pi}{2V_\pi}s(t)\right)\cdot\cos\left(\frac{\pi V_{bias}}{2V_\pi}\right)\right. \\ &\quad \left.-\sin\left(\frac{\pi}{2V_\pi}s(t)\right)\cdot\sin\left(\frac{\pi V_{bias}}{2V_\pi}\right)\right]\cos(2\pi f_c t) \end{aligned} \tag{4}$$

where V_π and V_{bias} are the half-wave voltage and the applied DC bias voltage to the MZM. f_c denotes the optical carrier frequency. $s(t)$ presents the electrical drive signal with a zero mean and a standard deviation of σ. From (1), the second-order Taylor series expansion with respect to $s(t)$ is given by

$$\begin{aligned} E_o(t) \propto &\left[\cos\left(\frac{\pi V_{bias}}{2V_\pi}\right)-\frac{1}{2}\cos\left(\frac{\pi V_{bias}}{2V_\pi}\right)\cdot\left(\frac{\pi}{2V_\pi}s(t)\right)^2\right. \\ &\left.-\frac{\pi}{2V_\pi}s(t)\cdot\sin\left(\frac{\pi V_{bias}}{2V_\pi}\right)\right]\cos(2\pi f_c t) \end{aligned} \tag{5}$$

For small σ, the second term may be neglected. Then, the optical carrier power (P_C) and the signal power (P_{DSB}) can be expressed as

$$P_C \propto \left|\cos\left(\frac{\pi V_{bias}}{2V_\pi}\right)\right|^2 \tag{6}$$

$$P_{DSB} \propto \left|\frac{\pi}{2V_\pi}\cdot\sigma\cdot\sin\left(\frac{\pi V_{bias}}{2V_\pi}\right)\right|^2 \tag{7}$$

The optical SSB-OFDM modulation is realized by optical filtering the optical DSB-OFDM signal with an optical band-pass filter. Therefore, the CSPR of the optical SSB-OFDM signal can be obtained by

$$\begin{aligned} CSPR &= 10\log_{10}\left(\frac{P_C}{P_{DSB}/2}\right) \\ &= 10\log_{10}\left(\frac{\left|\cos\left(\frac{\pi V_{bias}}{2V_\pi}\right)\right|^2}{\left|\frac{\pi}{2V_\pi}\cdot\sigma\cdot\sin\left(\frac{\pi V_{bias}}{2V_\pi}\right)\right|^2/2}\right) \end{aligned} \tag{8}$$

According to (8), the CSPR is related to the drive signal power and bias voltage, which can be reduced to an optimal one to improve the receiver sensitivity [3].

5. Simulation Setup

Due to our experimental limitations and further investigation of the proposed low-complexity receiver, the simulation setup of the guard-band SSB-DDO-OFDM transmission system is established as shown in Fig. 3. At the transmitter side, the pseudo-random binary sequence (PRBS) is first generated and mapped to 16-QAM symbols. Then, 999 Data-carrying SCs with indices from 1001 to 1999 are modulated with 16-QAM symbols. DC SC and 1000 low-frequency SCs are filled with zeroes to create the guard band. Other positive-frequency SCs are also filled with zeros for oversampling. The input vector of the inverse discrete Fourier transform (IDFT) in the transmitter is constrained to have Hermitian symmetry (HS). A 12-point cyclic prefix is added to the beginning of the real-valued IDFT outputs to resist the optical fiber dispersions. A single training sequence (TS) is inserted at

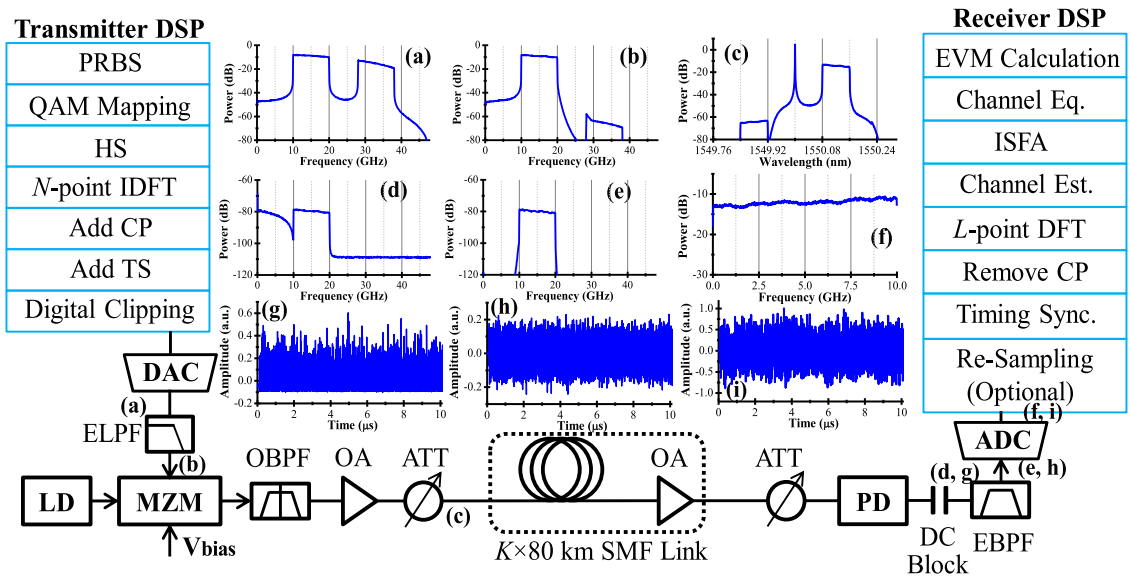

Fig. 3. Simulation setup including the representative spectral and waveforms.

the beginning of every OFDM frame and followed by 100 data-carrying OFDM symbols. The OFDM signal is digitally clipped before digital-to-analog conversion. The detailed parameters of the OFDM frame are the same as experimental measurements, as shown in Table 1. The clipped OFDM data is converted into the analog one by an 8-bit DAC worked at a sampling rate of 48 GS/s. The spectrum of the converted signal is shown in Fig. 3(a), where the spectrum roll-off is due to the DAC's zero-order-hold effect. A Chebyshev ELPF is added after the DAC to remove the high-frequency images. The spectrum of the filtered signal is presented in Fig. 3(b).

The filtered signal with a peak-to-peak voltage about 2 V, is modulated onto an optical carrier from a continuous wave laser diode (LD). The optical double-sideband OFDM signal is filtered by a Gaussian optical band-pass filter (OBPF) to realize OSSB modulation. The optical spectrum after the OBPF is shown in Fig. 3(c). An optical amplifier (OA) and an optical attenuation (ATT) are used to compensate the insertion loss of the MZM and fix the launch power at 8 dBm. The OSSB-OFDM is coupled into an optical fiber link which consists of K spans of 80 km of single-mode fiber (SMF) and K inline OAs for loss compensation. For simplification, the fiber nonlinearity isn't included in the simulations.

At the receiver end, an optical ATT is placed before PD to change the received optical power (ROP). The received electrical signal is directly-detected by the square-law PD. After DC block, the DC component of the received signal is removed. The corresponding power spectrum and time-domain waveform are shown in Fig. 3(d) and (g), respectively. As we can see clearly from Fig. 3(d), the guard band is fully filled with SSBI. And the time-domain waveform is asymmetrically clipped due to the square-law detection-induced SSBI. The desired OFDM signal is extracted after a Chebyshev electrical band-pass filter (EBPF), and its power spectrum and time-domain waveform are presented in Fig. 3(e) and (h), respectively. Fig. 3(h) shows that the waveform is symmetrical after removing SSBI. Subsequently, the desired signal is sampled at 20, 48, 96 and 192 GS/s for a comparison purpose.

For OFDM demodulation, the sampled data is first resampled when the sampling rate at 96 and 192 GS/s, and then realize timing synchronization using the known TS, CP removal, L-point DFT, TS-based and intra-symbol frequency averaging (ISFA)-enhanced channel estimation [20], single-tap channel equalization. At last, the EVM is calculated to evaluate the receiver performance. The detailed parameters used in the simulations are listed in Table 2. For different DC bias voltage applied to the MZM, optical fiber length and ADC resolution, the EVM performance comparisons

TABLE 2
Some Parameters Used in the Simulations

Item	Parameter	Value	Unit
DAC	Sampling rate	48	GS/s
	Resolution	8	bits
ADC	Sampling rate	20, 48, 96, 192	GS/s
	Resolution	4–10	Bits
	Filter type	Chebyshev	-
ELPF	Cutoff frequency	20	GHz
	Order	8	-
	Ripple factor	0.5	dB
	Operation wavelength	1550	nm
LD	Line-width	1	MHz
	Output power	10	dBm
MZM	Half-wave voltage ($V\pi$)	4	V
	Filter type	Gaussian	-
	Center wavelength	1550.09	nm
OBPF	BW	24	GHz
	Order	5	-
OA	Noise figure	4	dB
	Length	$K \times 80$ ($K = 0$–9)	km
	Attenuation	0.2	dB/km
SMF	Dispersion	17	ps/nm/km
	Dispersion slope	0.075	ps/nm^2/km
	Differential group delay	0.2	ps/km
	Responsivity	1	A/W
PD	Thermal noise	100e-24	W/Hz
	Dark current	10	nA
	Filter type	Chebyshev	-
	Center frequency	15	GHz
EBPF	BW	10.2	GHz
	Order	1–10	–
	Ripple factor	0.5	dB

between the proposed low-complexity receiver using ADC undersampling and the three conventional ADC oversampled guard-band SSB-DDO-OFDM receivers are performed.

6. Simulated Results and Discussions

6.1. CSPR Optimization

A low $\sigma = 0.2$ is used in this paper, and the simulated and theoretical CSPRs as a function of the ratio between the bias voltage and half-wave voltage are shown in Fig. 4. It shows that the simulated results are in good agreement with the theoretical results according to (8). When the V_{bias}/V_{π} is close to 0.965, the optimal CSPR (0 dB) will be achieved [3].

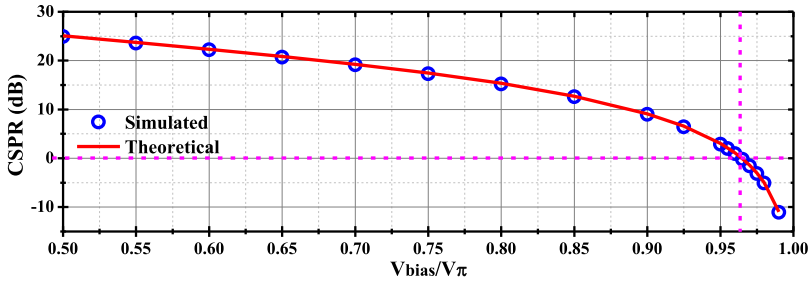

Fig. 4. CSPR versus the ratio of DC bias voltage to half-wave voltage of MZM.

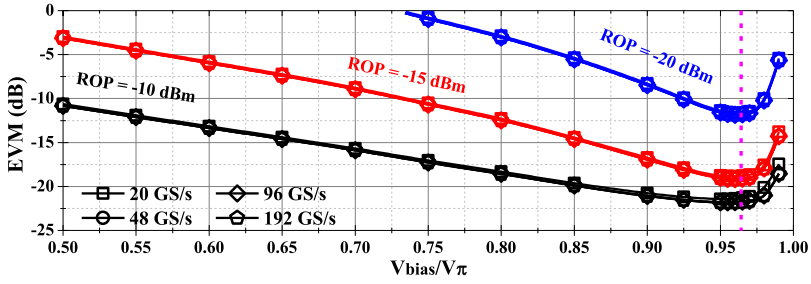

Fig. 5. EVM performance versus the ratio of DC bias voltage to half-wave voltage (8-bit ADC resolution and 8-th order EBPF).

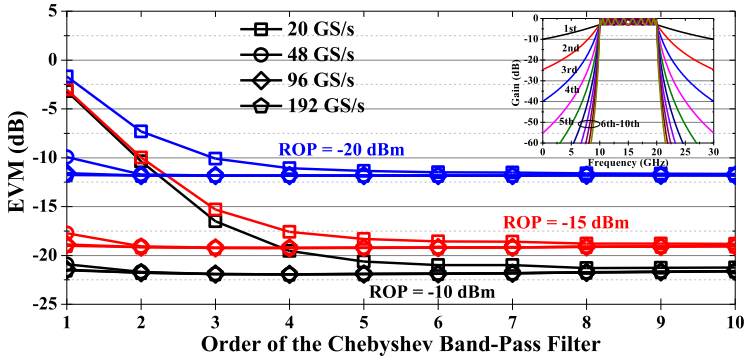

Fig. 6. EVM performance versus the order of the Chebyshev band-pass filter (8-bit ADC resolution).

The OSSB-OFDM signal after 320 km SMF transmission and the ADC resolution is 8-bit, then the EVM performances as a function of DC bias voltage at ROPs of −20, −15 and −10 dBm, are shown in Fig. 5. It indicates that the optimal DC bias voltage is about $0.965V_{\pi}$ in our simulations, and the proposed low-complexity receiver using undersampling at a sampling rate of 20 GS/s has the similar EVM performance as other three oversampling cases. It should be mentioned that the optimal DC bias voltage will be different when σ is changed. In practical applications, a larger drive signal may be used to avoid the large insertion loss of the MZM biased at a decreased DC voltage according to (8).

6.2. Electrical Band-Pass Filter Order Requirements

The proposed ADC sampling rate reduction method is sensitive to the residual SSBI, so the requirement of the EBPF order is necessary to be discussed. After the OSSB-OFDM signal after 320 km SMF transmission, the EVM performance versus the order of the Chebyshev band-pass filter is presented in Fig. 6. And the frequency responses of the 1^{st}–10^{th} order Chebyshev band-pass filter are also inserted in Fig. 6. For ROPs of −20, −15 and −10 dBm, the orders of the

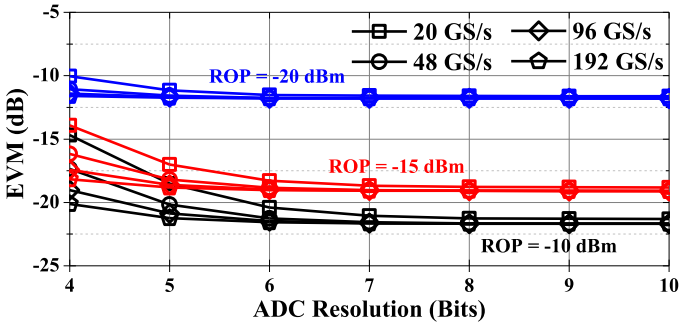

Fig. 7. EVM performance versus ADC resolutions (8-th order EBPF).

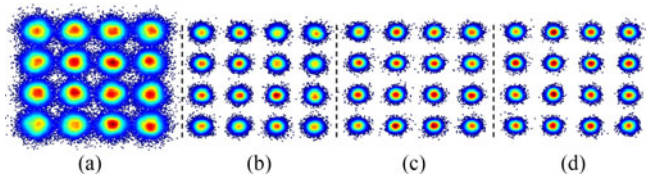

Fig. 8. Recovered 16-QAM constellation diagrams (a) 4-bit, 20 Gs/s, (b) 4-bit, 192 Gs/s, (c) 8-bit, 20 Gs/s, (d) 8-bit, 192 Gs/s.

EBPF are required to more than 4, 5 and 6, respectively, to achieve a negligible EVM performance degradation for the proposed method.

6.3. ADC Resolution Requirements

The undersampling technique can be used to relax ADC sampling rate and reduce the implementation complexity of the receiver. However, the receiver performance may be limited when ADC resolution is low, and quantization noise is dominant. It is very interesting to discuss the effects of ADC resolution on the receiver performance. Fig. 7 shows that the EVM performances after 320 km SMF transmission as a function of ADC resolution at ROPs of −20, −15 and −10 dBm. For the oversampled receiver with a 4-bit ADC worked at a sampling rate of 192 GS/s, the EVM performances are improved by 5.5, 4.2 and 1.6 dB when the ROPs are −10, −15 and −20 dBm, respectively, compared to the undersampled receiver. The undersampled receiver is limited by ADC quantization noise, while ADC oversampling can be applied to improve resolution and reduce quantization noise. However, the undersampled receiver has a similar EVM performance with other three oversampled receivers when the ADC with a resolution of 7-bits or more. The recovered16-QAM constellations with EVMs of −14.7, −20.2, −21.3 and −21.7 dB are presented in Fig. 8(a), (b), (c) and (d), respectively.

6.4. Sampling Clock Offset Tolerance

To investigate the sampling clock offset tolerance, a 256-time over-sampled signal is first generated. Samples at the desired instants due to sampling clock offset (SCO) between DAC clock in the transmitter and ADC clock in the receiver, which are then determined by a linear interpolation operation on the neighboring points [21]. The measured EVM performance as a function of the amount of the SCO is shown in Fig. 9. As a large IDFT size of 4800 is used in our simulations, the spectrum rolls off rapidly. Thus, the penalty induced by the interference between the positive-frequency band and negative-frequency band after undersampling in the presence of a small SCO, which is negligible. It exhibits that the two SSB-OFDM receivers are sensitive to SCOs in the same way. When the SCO is greater than 0.1 ppm, the EVM performance is dramatically degraded mainly due to the SCO-induced phase rotations. The corresponding constellations at an SCO of

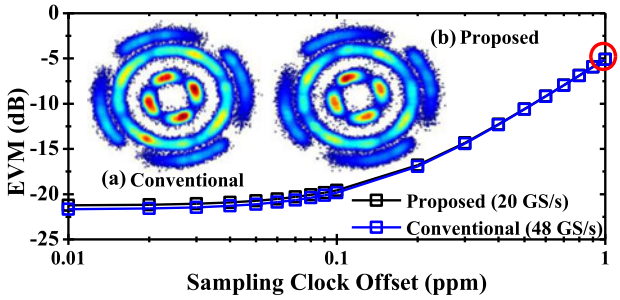

Fig. 9. EVM performance degradation versus sampling clock offset. (8-bit ADC resolution and 8-th order EBPF).

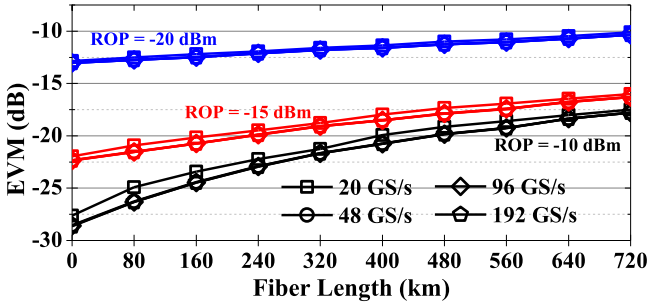

Fig. 10. EVM performance versus optical fiber length. (8-bit ADC resolution and 8-th order EBPF).

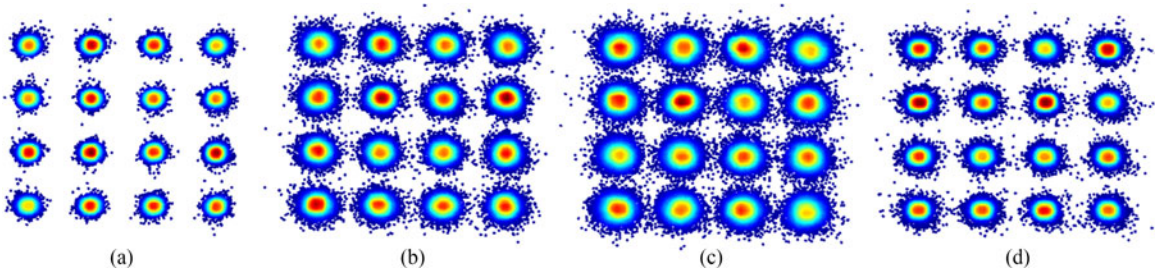

Fig. 11. Constellation diagrams after 160, 480 and 720 km SMF transmission. (a) 160 km SMF, LW = 1 MHz, EVM = −23.43 dB, (b) 480 km SMF, LW = 1 MHz, EVM = −19.15 dB, (c) 720 km SMF, LW = 1 MHz, EVM = −17.50 dB, (d) 720 km SMF, LW = 1 kHz, EVM = −21.81 dB.

1 ppm are inserted in Fig. 9(a) and (b). When SCO becomes large enough, the SCO-induced inter-channel interference (ICI) will significantly deteriorate the receiver performance in addition to the SCO-induced phase rotations. Several compensation methods have been reported for optical OFDM systems in the literature [18], [22]–[25].

6.5. Transmission Performance Over Fiber-Optic Links

The EVM performances as a function of optical fiber length at ROPs of −20, −15 and −10 dBm, are presented in Fig. 10. A similar EVM performance is also observed for the proposed undersampled receiver and three oversampled receivers. It is well known that laser phase noise will be converted into intensity noise by optical fiber dispersion [26]. When the line-width (LW) of the laser is 1 MHz, the 16-QAM constellation diagrams recovered by the proposed undersampled receiver after 160, 480 and 720 km SMF transmission are presented in Fig. 11(a), (b) and (c), respectively. Meanwhile, the constellation diagram after 720 km SMF transmission when the LW of the laser is 1 kHz, which is also plotted in Fig. 11(d). The corresponding EVM is −21.81 dB. It indicates that the degraded

EVM performance as optical fiber length increases is mainly attributed to the increased intensity noise in addition to the inline OA noise.

7. Conclusion

We propose a low-complexity receiver using ADC undersampling for the guard-band SSB-DDO-OFDM. Both the ADC sampling rate and DFT size are reduced by more than half. Thus, the implementation complexity of the receiver can be greatly reduced with the lower ADC sampling rate and reduced digital signal processing (DSP) complexity. The simulations show that the proposed undersampled receiver has the same EVM performances as the oversampled receivers when ADC quantization noise is not dominant. We believe that the proposed guard-band SSB-DDO-OFDM has several advantages such as simple system configuration, high receiver sensitivity and low DSP complexity, may be more suitable for the hardware implementation.

References

[1] A. J. Lowery, D. Liang, and J. Armstrong, "Orthogonal frequency division multiplexing for adaptive dispersion compensation in long haul WDM systems," in *Proc. 2006 Opt. Fiber Commun. Conf./Nat. Fiber Opt. Eng. Conf.*, 2006, Paper PDP39.

[2] B. J. C. Schmidt, A. J. Lowery, and J. Armstrong, "Experimental demonstrations of electronic dispersion compensation for long-haul transmission using direct-detection optical OFDM," *J. Lightw. Technol.*, vol. 26, no. 1, pp. 196–203, Jan. 2008.

[3] A. Ali, J. Leibrich, and W. Rosenkranz, "Spectral efficiency and receiver sensitivity in direct detection optical-OFDM," in *Proc. Opt. Fiber Conf.*, 2009, Paper OMT7.

[4] Z. Cao, J. Yu, W. Wang, L. Chen, and Z. Dong, "Direct-detection optical OFDM transmission system without frequency guard band," *IEEE Photon. Technol. Lett.*, vol. 22, no. 11, pp. 736–738, Jun. 2010.

[5] F. Li, X. Li, L. Chen, Y. Xia, C. Ge, and Y. Chen, "High-level QAM OFDM system using DML for low-cost short reach optical communications," *IEEE Photon. Technol. Lett.*, vol. 26, no. 9, pp. 941–944, May 2014.

[6] R. Bouziane *et al.*, "Experimental demonstration of 30 Gb/s direct-detection optical OFDM transmission with blind symbol synchronisation using virtual subcarriers," *Opt. Exp.*, vol. 22, no. 4, pp. 4342–4348, 2014.

[7] X. Q. Jin, E. Hugues-Salas, R. P. Giddings, J. L. Wei, J. Groenewald, and J. M. Tang, "First real-time experimental demonstrations of 11.25 Gb/s optical OFDMA PONs with adaptive dynamic bandwidth allocation," *Opt. Exp.*, vol. 19, no. 21, pp. 20557–20570, 2011.

[8] M. Chen, J. He, Q. Fan, Z. Dong, and L. Chen, "Experimental demonstration of real-time high-level QAM-Encoded direct-detection optical OFDM systems," *J. Lightw. Technol.*, vol. 33, no. 22, pp. 4632–4639, Nov. 2015.

[9] F. Li, X. Xiao, X. Li, and Z. Dong, "Real-time demonstration of DMT-based DDO-OFDM transmission and reception at 50 Gb/s," in *Proc. 39th Eur. Conf. Exhib. Opt. Commun.*, 2013, Paper 6.2.

[10] S.-H. Cho, K. W. Doo, J. H. Lee, J. Lee, S. I. Myong, and S. S. Lee, "Demonstration of a real-time 16 QAM encoded 11.52 Gb/s OFDM transceiver for IM/DD OFDMA-PON systems," in *Proc. 18th OptoElectron. Commun. Conf./2013 Int. Conf. Photon. Switching*, 2013, Paper WP2-3.

[11] C. Xu, M. Wang, Y. Song, and L. Yu, "High-speed real-time optical OFDM transmission system based on asynchronous clock," in *Proc. Asia Commun. Photon. Conf.*, 2013, Paper AF2F.59.

[12] Q. W. Zhang *et al.*, "Record-high and robust 17.125 Gb/s gross-rate over 25 km SSMF transmissions of real-time dual-band optical OFDM signals directly modulated by 1 GHz RSOAs," *Opt. Exp.*, vol. 22, no. 6, pp. 6339–6348, 2014.

[13] M. Schuster, C. A. Bunge, B. Spinnler, and K. Petermann, "120 Gb/s OFDM transmission with direct detection using compatible single-sideband modulation," in *Proc. Opt. Fiber Conf.*, 2008, Paper OMU7.

[14] W.-R. Peng *et al.*, "Theoretical and experimental investigations of direct-detected RF-tone-assisted optical OFDM systems," *J. Lightw. Technol.*, vol. 27, no. 10, pp. 1332–1339, May 2009.

[15] J. Ma, "Simple signal-to-signal beat interference cancellation receiver based on balanced detection for a single-sideband optical OFDM signal with a reduced guard band," *Opt. Lett.*, vol. 38, no. 21, pp. 4335–4338, 2013.

[16] S. Alireza Nezamalhosseini, L. R. Chen, Q. Zhuge, M. Malekiha, F. Marvasti, and D. V. Plant, "Theoretical and experimental investigation of direct detection optical OFDM transmission using beat interference cancellation receiver," *Opt. Exp.*, vol. 21, no. 13, pp. 15237–15246, 2013.

[17] R. A. Shafik, S. Rahman, and R. Islam, "On the extended relationships among EVM, BER and SNR as performance metrics," in *Proc. Int. Conf. Elect. Comput. Eng.*, 2006, pp. 408–411.

[18] M. Chen, J. He, J. Tang, and L. Chen, "Pilot-aided sampling frequency offset estimation and compensation using DSP technique in DD-OOFDM systems," *Opt. Fiber Technol.*, vol. 20, no. 3, pp. 268–273, 2014.

[19] J. Leibrich, A. Ali, H. Paul, W. Rosenkranz, and K. D. Kammeyer, "Impact of modulator bias on the OSNR requirement of direct-detection optical OFDM," *IEEE Photon. Technol. Lett.*, vol. 21, no. 15, pp. 1033–1035, Aug. 2009.

[20] X. Liu and F. Buchali, "Intra-symbol frequency-domain averaging based channel estimation for coherent optical OFDM," *Opt. Exp.*, vol. 16, no. 26, pp. 21944–21957, 2008.

[21] H. Shafiee, B. Nourani, and M. Khoshgard, "Estimation and compensation of frequency offset in DAC/ADC clocks in OFDM systems," in *Proc. IEEE Int. Conf. Commun.*, 2004, pp. 2397–2401.

[22] X. Q. Jin and J. M. Tang, "Optical OFDM synchronization with symbol timing offset and sampling clock offset compensation in real-time IMDD systems," *IEEE Photon. J.*, vol. 3, no. 2, pp. 187–196, Apr. 2011.
[23] R. Deng, J. He, M. Chen, and L. Chen, "SFO compensation by pilot-aided channel estimation for real-time DDO-OFDM system," *Opt. Commun.*, vol. 355, pp. 172–176, 2015.
[24] X. Yi and K. Qiu, "Estimation and compensation of sample frequency offset in coherent optical OFDM systems," *Opt. Exp.*, vol. 19, no. 14, pp. 13503–13508, 2011.
[25] M. Chen, J. He, Z. Cao, J. Tang, L. Chen, and X. Wu, "Symbol synchronization and sampling frequency synchronization techniques in real-time DDO-OFDM systems," *Opt. Commun.*, vol. 326, pp. 80–87, 2014.
[26] A. Gatto, S. Mandelli, J. Morosi, M. Magarini, P. Martelli, and P. Boffi, "Experimented phase noise limitations in directly-detected single side-band optical OFDM systems," in *Proc. Opt. Fiber Conf.*, 2017, Paper Th2A.29.